JOURNAL OF Applied Polymer SCIENCE

Poly(vinylidene fluoride)/Halloysite Nanotubes Nanocomposites: The Structures, Properties, and Tensile Fracture Behaviors

Xue-Gang Tang,[1] Meng Hou,[1] Jin Zou,[1,2] Rowan Truss[1]

[1]School of Mechanical and Mining Engineering, The University of Queensland, Brisbane, Queensland 4072, Australia
[2]Centre for Microscopy and Microanalysis, The University of Queensland, Brisbane, Queensland 4072, Australia
Correspondence to: M. Hou (E-mail: m.hou@uq.edu.au)

ABSTRACT: Poly(vinylidene fluoride)/halloysite nanotubes (HNTs) nanocomposites with good dispersion were prepared. The effect of HNTs on the crystalline structure, dynamic rheological properties, dynamic mechanical properties, and tensile properties was investigated. Results showed that at low concentration, the effect of HNTs on the modulus was minor. However, at high concentration, improvement of the modulus can be observed. The tensile fracture behaviors were investigated, which showed that the addition of HNTs changed the fracture mode. When the concentration of HNTs was 20 phr, a fracture mode change from microductility/brittle to brittle/fibrillation occurred. © 2012 Wiley Periodicals, Inc. J. Appl. Polym. Sci. 000: 000–000, 2012

KEYWORDS: composites; structure-property relations; mechanical properties

Received 10 April 2012; accepted 24 June 2012; published online
DOI: 10.1002/app.38249

INTRODUCTION

Polymer matrices reinforced by nanofillers have attracted considerable attention in recent years due to their higher mechanical, thermal, and physical properties. Different types of nanofillers, like clay, carbon nanotubes etc. have been used.[1–10] Comparing with other nanosized inorganic fillers, naturally occurring halloysite nanotubes (HNTs) are readily available and much cheaper. More importantly, the unique crystal structure of HNTs, such as rod-like geometry and low hydroxyl density on the surface, makes them readily dispersed in a polymer matrix.[11] This makes high concentration of nanofillers with good dispersion possible and offers great opportunities for fabricating polymer nanocomposites with promising performance.

Ye et al.[12] prepared epoxy-based nanocomposites with natural nanotubes from halloysite. Results showed the HNTs were geometrically similar to multiwalled carbon nanotubes, and the blending of epoxy with 2.3 wt % HNTs increased the impact strength by four times without scarifying flexural modulus, strength, and thermal stability. Liu et al.[11] formed organic–inorganic hybrids with epoxy/cyanate ester resin and HNTs. The dispersion of HNTs in the resin matrix was very uniform. Results showed that the moduli of the hybrids in the glassy state and rubbery state were significantly higher than those for the plain cured resin. For instance, the glassy and rubbery moduli of the hybrid with 12 wt % HNTs were 58.6 and 121.7% higher than those of the neat epoxy resin, respectively. Ning et al.[13] prepared polypropylene (PP)/halloysite composites by melt mixing using a twin-screw extruder. Results revealed that HNTs were well-dispersed in PP matrix and had a good interfacial interaction with PP. However, not much enhancement in mechanical properties of PP/HNT composites had been achieved, which was ascribed to the constant crystallinity and spherulite size of PP as well as the small length/diameter ratio of HNTs. Liu et al.[14] used 2,5-bis(2-benzoxazolyl) thiophene (BBT) as the interfacial modifier for PP/HNTs composites. The electron transfer between HNTs and BBT was confirmed. Formation of fibrils of BBT in the presence of HNTs was found in the nanocomposites, which led to much higher crystallinity compared with previously reported PP nanocomposites. The nanocomposites showed substantially increased tensile and flexural properties. For example, the tensile strength increased from 33.2 to 38.8 MPa, flexural strength from 41.8 to 61.4 MPa, and flexural modulus from 1.24 GPa to 2.83 GPa. Pasbakhsh et al.[15] investigated the influence of maleic anhydride-grafted ethylene propylene diene monomer (MAH-*g*-EPDM) on the properties of EPDM nanocomposites reinforced by HNTs. Results showed that hydrogen bonding occurred between MAH-*g*-EPDM and HNTs. Morphological observations revealed the formation of two different phases of EPDM-rich and HNT rich areas. Tensile strength was increased from 1.32 MPa to about 12 MPa.

Poly(vinylidene fluoride) (PVDF) is an important engineering plastic with applications in such diverse fields as paint for skyscrapers, transducers for sensitive scientific instruments, and

Table I. Samples Codification

Sample	Composition
PVDF	PVDF (100 phr)
PH_2	PVDF (100 phr) + HNTs (2 phr)
PH_5	PVDF (100 phr) + HNTs (5 phr)
PH_{10}	PVDF (100 phr) + HNTs (10 phr)
PH_{20}	PVDF (100 phr) + HNTs (20 phr)

pipes for caustic chemical products.[16,17] Our previous research showed that PVDF has high potential application in the thermoset composite welding (TCW) technology. The world-class international patented technology showed its advantage for cost saving in the joining and repairing of composite materials and represents the "Next-Generation" assembly technology for aerospace composite structures.[18] The incorporation of HNTs into PVDF has the potential to improve the performance for PVDF and therefore benefit TCW technology. However, as far as we know, to date there are no reports of work on PVDF/HNTs nanocomposites.

In this research, PVDF/HNTs nanocomposites with different concentration of HNTs were fabricated. Systematic studies about the effect of the HNTs on the morphological structures, crystalline structures, rheological properties, mechanical properties were investigated. The tensile fracture behavior was also investigated.

EXPERIMENTS

Materials

PVDF (Kynar 741, powder) was kindly supplied free-of-charge by Arkema (Australia, New Zealand). The HNTs (HNTs) were kindly supplied free-of-charge by Imerys Tableware New Zealand (Ultrafine, Castle Hill, New South Wales, Australia). Analytical grade *N*-methyl-2-pyrrolidone (NMP) purchased from Aldrich was used as solvent. All chemicals were used as received.

Preparation of the Nanocomposites

The procedure for the fabrication of nanocomposites was as follows: (1) HNTs were dispersed in solvent NMP with strong mechanical stirring and ultrasonic treatment (60 kHz, 1.5 h). At the same time, the polymer, PVDF, was dissolved in NMP to form PVDF solution (the ratio of PVDF and solvent was 1 : 5 by weight); (2) The HNTs dispersion and the PVDF solution were mixed together again with strong magnetic stirring and ultrasonic treatment (1.5 h); (3) The mixed solution was poured onto a glass plate and then compressed with another glass plate; (4) the glass plates were placed into deionized water (the anti-solvent to NMP), which caused the film to solidify in 3–5 min. The wet films were then dried in a vacuum oven for 72 h at 80°C to remove any remnant of the solvent. The dried nanocomposites films were then compression molded using a matched metal die in a hot press at 200°C and 5.0 MPa pressure. The compression molded nanocomposites sheets were used for testing and subsequently characterization.

As summarized in Table I, various blend formulations were prepared.

Characterization

Transmission electron microscopy (TEM) images of the prepared nanocomposites were obtained using a JEOL 1010A high-resolution transmission electron microscope operated at 100 kV. A Reichert-Jung Ultracut-E microtome was used to cut thin sections out of nanocomposites sheets with thickness of 50–70 nm for TEM characterization.

Scanning electron microscopy (SEM) was performed on a JEOL JSM-6300F scanning electron microscope at a voltage of 6 kV. Samples were sputter-coated with a 10 nm-thick layer of platinum before imaging.

DSC tests were conducted by means of a TA Q20 differential scanning calorimeter. In the tests, samples of about 5 mg were heated to 200°C at a rate of 10°C/min under a nitrogen atmosphere and held at 200°C for 5 min to eliminate the thermal

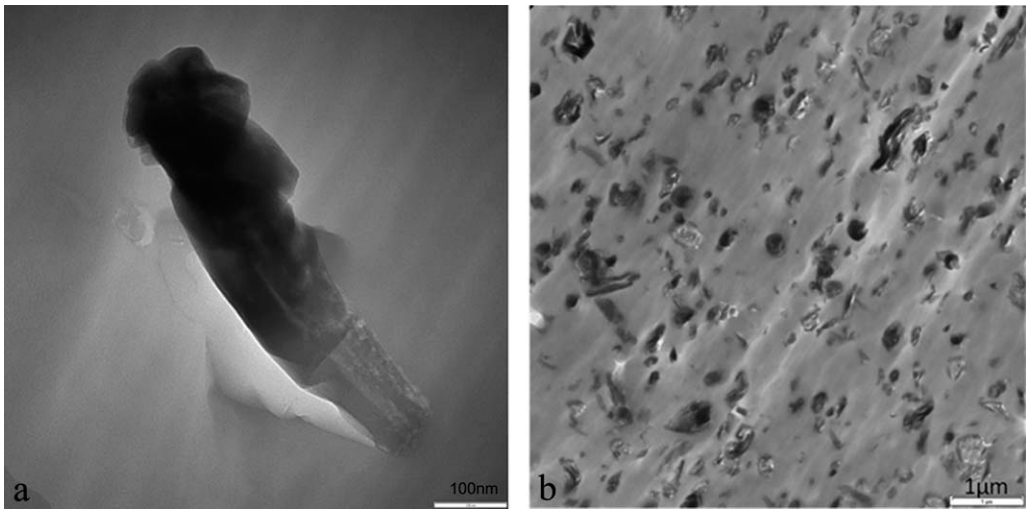

Figure 1. TEM image of PVDF/HNTs nanocomposits: (a) single HNT, (b) PH_{20}.

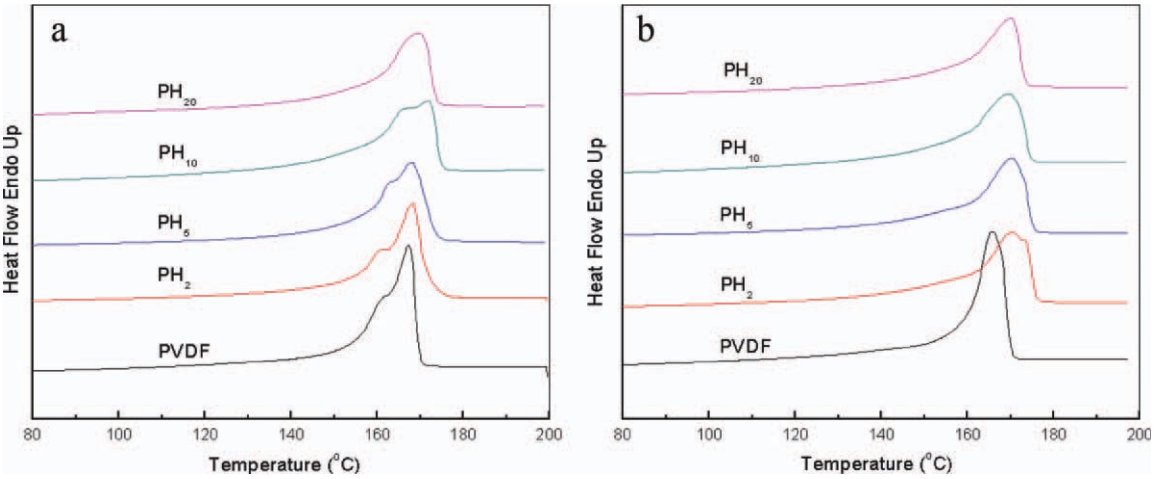

Figure 2. Nonisothermal DSC scans of PVDF and its nanocomposites. (a) first heating round, (b) second heating round. [Color figure can be viewed in the online issue, which is available at wileyonlinelibrary.com.]

history. Afterward, the samples were cooled to 20°C at a rate of 20°C/min, held at 20°C for about 3 min, and then heated again to 200°C at a heating rate of 10°C/min. The temperature and heat flow scales were calibrated using the melting of high-purity indium and zinc samples before testing.

ATR FTIR spectrum was obtained using a Nicolet 5700 ART spectrometer with an average of 200 scans in the range 400–2000 cm^{-1} to obtain crystal structural for the nanocomposites.

Rheological measurements were performed using a TA AR2000 EX stress-controlled rheometer in parallel plate geometry at 200°C. The testing samples in the form of disk with a thickness of 1.5 mm and a diameter of 25 mm were prepared by compression molding at 200°C. Small-amplitude oscillatory shear measurements were conducted within a frequency range from 0.01 to 100 Hz. A sinusoidal strain of the form

$$\gamma(t) = \gamma_0 \sin(\omega t)$$

where γ_0 is strain amplitude, ω is oscillatory frequency, and t is time was imposed on the testing samples. The viscoelastic parameters, storage modulus G′, and loss modulus G″ of the samples were recorded. All the tests were performed under nitrogen environment to minimize oxidative degradation.

The dynamic mechanical analysis (DMA) (tension deformation) was carried out using a TA Instruments Q800 DMA. All the samples (30 × 4 mm^2) were measured over a temperature range of −100°C to 150°C at a heating rate of 3°C/min and a frequency of 1 Hz. To guarantee the reliability of the connected data, the test machine was calibrated according to the recommended standard before the test, and then three PVDF samples were tested, and results showed pretty good repeatability.

The mechanical properties of all materials were measured by an Instron 5584 universal testing machine with a 100 N load cell at a crosshead velocity of 5 mm/min until failure. Dumbbells were punched out of the nanocomposites sheets according to ASTM D-638 (the width is about 2.5 mm, video gauge is about 10 mm, and thickness is about 0.5 mm), and tests were carried out at 23°C. The tensile strength used is the tensile strength at yield, and the calculation of the Young's modulus is according to the standard using the almost linear initial part of the curve.

RESULTS AND DISCUSSION

Morphology of the Nanocomposites

Representative images of nanocomposites are shown in Figure 1. It was observed that the diameter for HNTs was around 50–100 nm, and the length was around 100–600 nm, which made the aspect ratio quite small for HNTs used in this work. However, it was observed that the HNTs were almost homogeneously dispersed in the PVDF matrix, even at the high concentration of 20 phr. Several factors are believed to contribute to the fine dispersion of HNTs in the PVDF matrix: First, it is known that the solution blending method is an easy way to achieve fine dispersion, especially with ultrasonic treatment and magnetic stirring. Second, the unique rod-like crystal structure of HNTs, and the low hydroxyl density on the surface, makes them readily

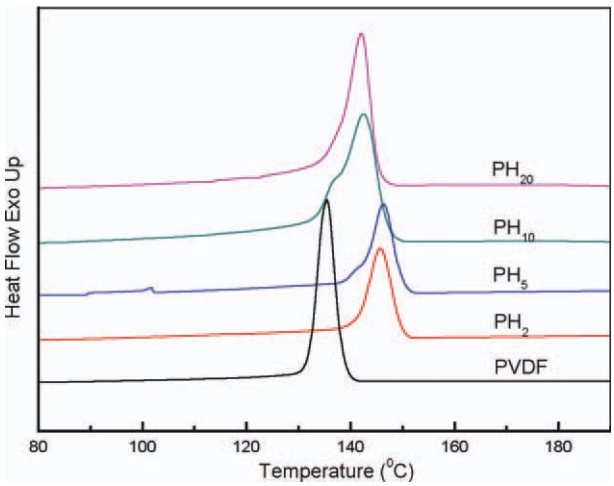

Figure 3. Crystallization DSC curves for PVDF and its nanocomposites. [Color figure can be viewed in the online issue, which is available at wileyonlinelibrary.com.]

Table II. DSC Parameters of PVDF and Its Nanocomposites (Normalized)

Sample	ΔH_m(J/g)		T_m(°C)		ΔH_c (J/g)	T_c (°C)
	First heating	Second heating	First heating	Second heating		
PVDF	42.20	44.87	167.29	165.71	47.71	135.47
PH_2	39.93	40.16	168.68	170.66	36.99	146.67
PH_5	40.96	42.66	168.09	170.34	35.89	146.35
PH_{10}	42.57	44.69	172.06	169.71	38.75	142.56
PH_{20}	44.11	46.79	169.62	170.25	38.29	142.08

dispersible in a hydrophobic polymer matrix. Especially here, the hydroxyl group on the surface of HNTs may interact with the polar solvent, NMP, which will help the dispersion of the HNTs in the solvent, and hence the formation of a stable suspension. Third, the fast phase separation method used in this research can avoid the drawback of the traditional solvent casting method, which needs much longer times to evaporate the solvent and may result in reagglomeration during evaporation.

Crystallization Behavior and Crystal Structure

Typical DSC heating and cooling curves are plotted in Figures 2 and 3, and the corresponding data are summarized in Table II, in which the enthalpy has been normalized according to the net weight of PVDF matrix in the nanocomposites. With the addition of 2 phr HNTs, the crystallization temperature (T_c) increased significantly. The increase of the crystallization temperature is due to the nucleating effect of HNTs during the crystallization process. However, crystallization enthalpy (ΔH_c) decreased significantly. With the HNTs concentration increasing further, the T_c decreased further, and a minor variance of ΔH_c occurred. Another interesting phenomenon is that an obvious low temperature shoulder on the crystallization peak occurred for sample PH_{10}, the position of which is close to the crystallization temperature for pure PVDF. At the same time, it was observed that an obvious low temperature shoulder was present on the first melting curve for the pure PVDF and for all of the nanocomposites. However, it was much less prominent in the second melting curve, which showed that this peak is associated with the heating history. It is interesting that the intensity of the lower melting peak increased with the addition of HNTs, and at the highest amount (20 phr), the lower one and the higher one merged together and formed a single peak. The ΔH_m and equilibrium melting temperature (T_m) showed a minor variance with the addition of HNTs.

To verify the crystal structures of PVDF and its nanocomposites, ATR-FTIR was conducted, and the result is shown in Figure 4. The α-phase PVDF bands at 974, 795, and 764 cm^{-1} can be clearly observed in pure PVDF. There was a small peak peat at 840 cm^{-1} for pure PVDF, which is common for both γ- and β-phases; however, it is obvious that the α-phase is the dominated phase. With the addition of HNTs, the intensity of the peat at about 840 cm^{-1} increased with a decrease of the peaks for the α-phases, indicating a change in the crystalline morphology.[17] At the same time, a shoulder peak at 812 cm^{-1}, which is specific to γ-phase,[19] can be observed for the nanocomposites except for PH_{20}.Thus, in this research, the addition of HNTs was seen to promote the crystallization of the γ-phase. The γ-phase increased with increasing HNTs amount, but reached a maximum at the HNTs concentration of 10 phr, and then sharply decreased so that the γ-phase almost disappeared at the HNTs concentration of 20 phr.

Dynamic Oscillatory Response

Figure 5 shows the storage modulus and loss modulus of PVDF and its nanocomposites with the introduction of HNTs. Many reports of polymer nanocomposites show that a strong enhancement in the elasticity (plateau modulus) occurs with the introduction of nanofillers. As indicated in Figure 5, the qualitative features (shapes) of the viscoelastic behavior were not affected by the introduction of the HNTs, even at the HNTs concentration of 20 phr. However, at a quantitative level, the introduction of HNTs resulted in an increase in the magnitudes of the storage modulus and loss modulus, especially for the sample PH_{20} where a significant increase occurred.

Pryamitsyn and Ganesan[20] studied the mechanisms governing the linear viscoelasticity behavior of nanocomposites of spherical nanofillers dispersed in polymer melts by computer simulation and several mechanisms have been put forward to explain the enhancement of the elasticity: one is that the particles

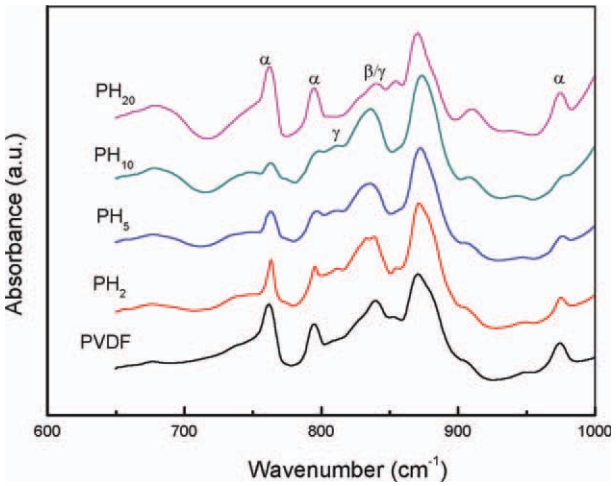

Figure 4. ART-FTIR spectra of PVDF and its CNTs nanocomposites. [Color figure can be viewed in the online issue, which is available at wileyonlinelibrary.com.]

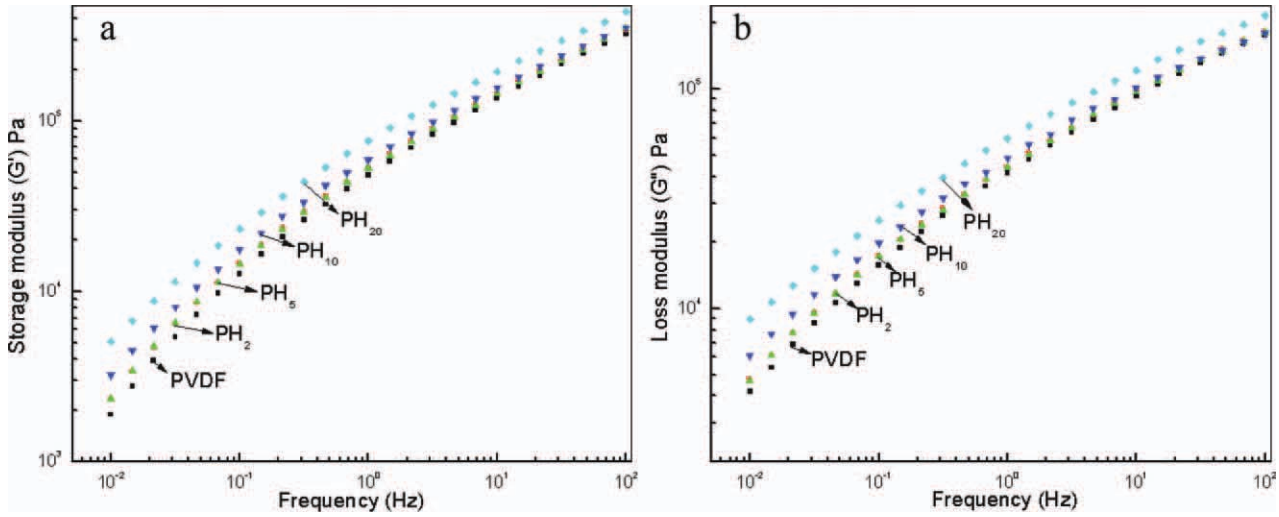

Figure 5. Log–log plots of dynamic moduli versus frequency for PVDF and its nanocomposites: storage modulus (a) and loss modulus (b). [Color figure can be viewed in the online issue, which is available at wileyonlinelibrary.com.]

induce effects on the dynamics of polymer segments that modify the relaxation spectrum of the polymers; another is that particle jamming effects lead to slow relaxations and substantial enhancements in elasticity; and the third is that the strain field distortion caused by the presence of rigid inclusions affects the overall modulus of the composite. From the TEM in Figure 1, it was observed that the aspect ratio of the HNTs used here was small, and the particle jamming effects would be expected to be weak. Therefore even at a concentration of 20 phr, no obvious solid-like behavior at low frequency regimes occurred. The nanofillers were seen to induce effects on the dynamics of polymer segments and modify the relaxation spectrum of the polymers. The restricted molecular mobility due to hydrodynamic effects of the nanofillers could be followed by the crossover point characteristic at which the values of G′ and G″ are equal. The shift in crossover frequency represents the changes in molecular mobility and relaxation behavior.[21] Table III shows the crossover frequency and the crossover modulus. It was observed that with the introduction of HNTs, the crossover frequency decreased.

Dynamic Mechanical Behavior

Figure 6 shows the DMA results of PVDF and its nanocomposites. It was observed that at low concentration (2, 5 phr) the addition of HNTs did not affect the storage modulus significantly. However, when the concentration increased to 10 and 20 phr, a significant increase in the storage modulus occurred, which showed the reinforcement effect of the HNTs. The tan δ curves of PVDF and its nanocomposites showed a broad peak near −30°C, which corresponds to the T_g of PVDF. No significant variation in the T_g was observed with the addition of HNTs, even for the sample at the highest concentration of 20 phr, indicating no significant variation in the mobility of PVDF molecule chains. However, the other relaxation peaks were affected significantly by the addition of HNTs. The relaxation peak at about 25°C for PVDF, which should belong to the α_2 transition related to the amorphous region at the surfaces of crystals,[22,23] increased with 2 phr HNTs content and then droped with increasing HNT content. The relaxation peak (α_1) at about 90°C, which is assigned to the liberation of PVDF chains in the crystalline regions,[24] shifted to a lower temperature (about 70°C) with the addition of HNTs and almost disappeared at the highest concentration of HNTs (20 phr). This is due to the addition of HNTs affected the crystalline structures, which showed significant changes tested by DSC with the introduction of HNTs.

Tensile Behavior

To determine the mechanical properties of PVDF and its nanocomposites, tensile measurements were carried out. Typical stress–strain curves at 5 mm/min for PVDF and its nanocomposites are shown in Figure 7, and the mechanical properties calculated from the stress–strain curves are shown in Table IV.

It was observed that the Young's modulus increased with the addition of HNTs. At the highest concentration (20 phr) about 56% improvement occurred. For the tensile strength, a minor decrease was observed with the increasing HNTs concentration. The decrease in the tensile strength can be regarded as the result of the weak interfacial adhesion between PVDF matrix and HNTs nanofiller, which would make the debonding and slippage between the matrix and nanofillers easy. Neat PVDF exhibits distinct regions such as yielding and plastic deformation. After yielding, further tensile deformation resulted in specimen

Table III. The Crossover Frequency and Crossover Modulus for PVDF and Its Nanocomposites

Sample	Crossover frequency (Hz)	Crossover modulus (Pa)
PVDF	0.33	2.71×10^4
PH_2	0.26	2.62×10^4
PH_5	0.26	2.58×10^4
PH_{10}	0.21	2.71×10^4
PH_{20}	0.16	3.06×10^4

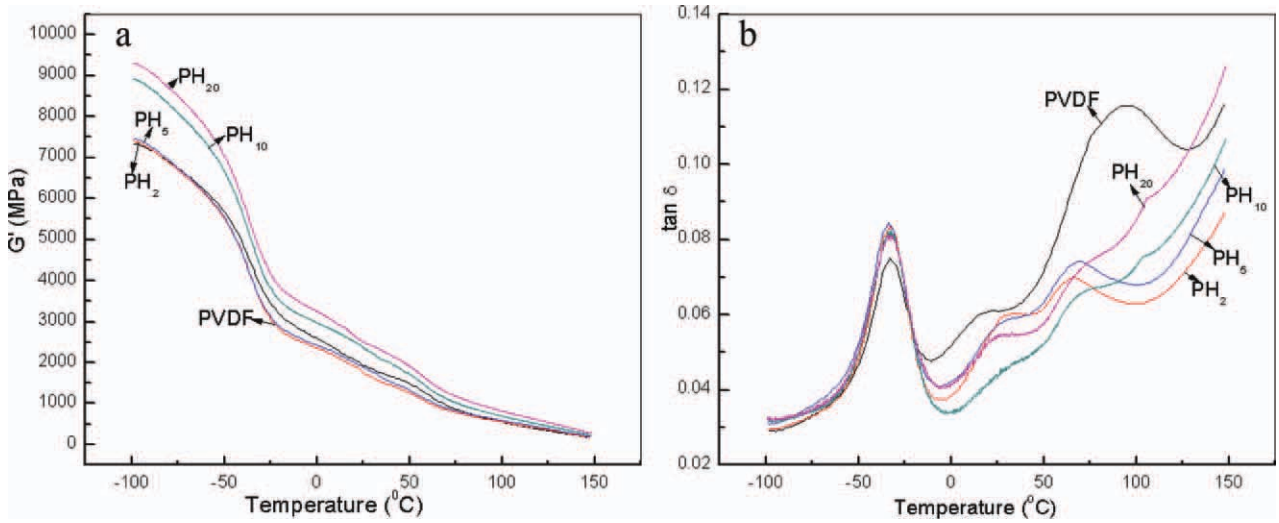

Figure 6. DMA test for PVDF and its nanocomposites. (a) storage modulus, (b) tan δ. [Color figure can be viewed in the online issue, which is available at wileyonlinelibrary.com.]

necking and cold drawing. The neck propagated along the gauge length exhibiting cold drawing until the specimen failed. With the addition of HNTs, at low concentration (2 phr, 5 phr), similar stress–strain curves were observed. For sample PH_{10}, much less cold drawing was observed. However, when the concentration of HNTs reached 20 phr, just yielding and the start of necking was observed, the stress–strain plots did not exhibit cold drawing. It was obvious that there was a transition in the failure behavior with the HNTs concentration increasing. To study the mechanism for the transition, the fracture morphology was investigated.

Fracture Morphology

Neat PVDF. Figure 8 shows the tensile-fractured surface morphologies of virgin PVDF at different magnifications. Macroscopically, the fractured surface can be classified as two parts, one was the microductility at the edges and the other was the brittle mode of fracture in the center. At higher magnification, one can observed that the brittle part presented large flat area with zig-zag steps [Figure 8(c)], which is due to the crack propagating on slightly different planes and these planes have to link up at some points and it leaves a step on the surface.[25] In the microductility region, sample presented large plastic deformation feature [Figure 8(d)]. It can be deduced that the fracture starts near the core of the sample and propagates outwards breaking through the ductile surface. Similar results have been reported by Misra and coworkers[26–28] and Shi et al.[29] The explanation for the microductility fracture at the edges is that a transition to plane stress occurred with the propagation of the fracture from the core to the edges.

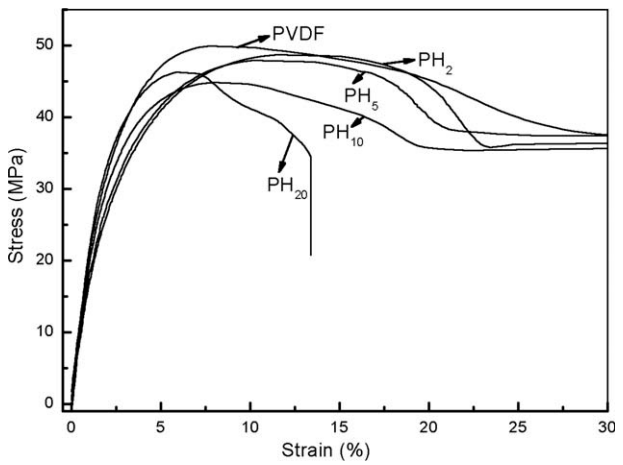

Figure 7. Typical stress–strain curves of PVDF and its nanocomposites.

PH_{10}

Figure 9 shows the tensile-fractured surface morphologies of PVDF nanocomposites with 10 phr HNTs at different magnifications. Macroscopically, the fractured surface was similar to the virgin PVDF, again showing, microductility at the edges and the brittle mode of fracture in the center. However, at higher magnification, differences can be observed. For virgin PVDF, the brittle area presented flat with zig-zag steps morphology. For PH_{10}, large amount of voids appeared. For virgin PVDF, the microductility region showed smooth surface, whereas PH_{10} presented pretty rough surface. This is due the changes of the distribution of local stress by the appearance of HNTs.

Table IV. Mechanical Properties from Tensile Testing for PVDF and Its Nanocomposites[a]

Sample	Young's modulus (GPa)	Tensile strength (MPa)	Elongation at break (%)
PVDF	1.97 (0.05)	50.0 (0.3)	254 (121)
PH_2	2.18 (0.09)	48.0 (0.4)	239 (64)
PH_5	2.40 (0.28)	48.0 (0.5)	213 (28)
PH_{10}	2.37 (0.11)	45.8 (1.0)	102 (26)
PH_{20}	3.08 (0.16)	45.7 (0.5)	10 (3)

[a]The data are mean value followed (in parentheses) by the standard deviation.

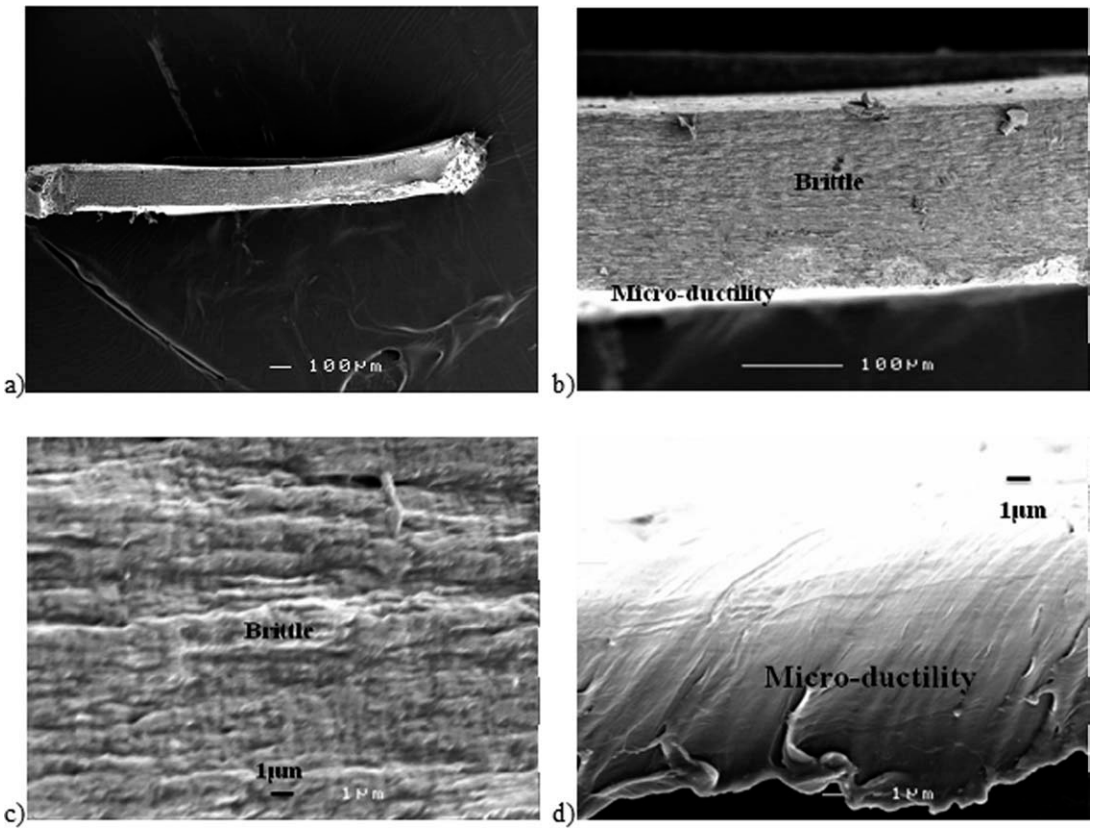

Figure 8. SEM micrograph of the fracture of neat PVDF: (a) low magnification; (b) high magnification; (c) brittle; (d) microductility.

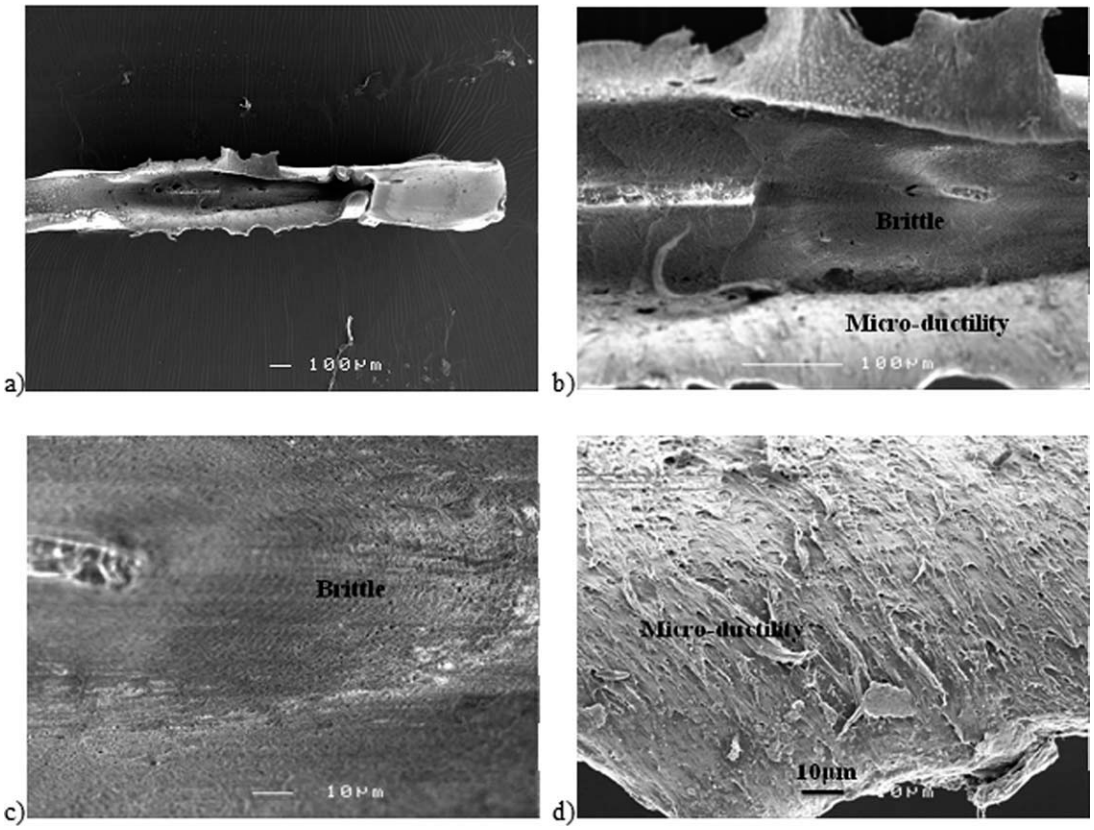

Figure 9. SEM micrograph of the fracture of neat PH_{10}: (a) low magnification; (b) high magnification; (c) brittle; (d) microductility.

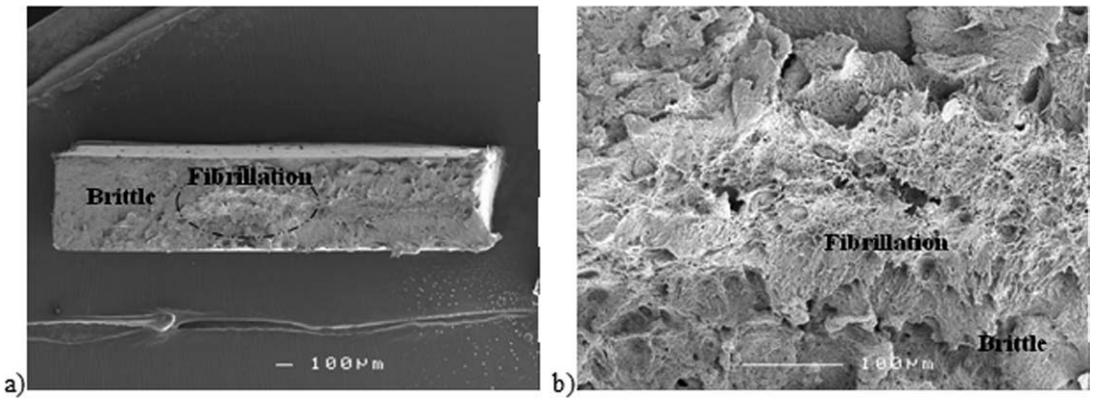

Figure 10. SEM micrograph of the fracture of neat PH_{20}: (a) low magnification; (b) high magnification in the fibrillation area.

PH_{20}. Figures 10 and 11 show the tensile-fractured surface morphologies of PVDF nanocomposites with 20 phr HNTs. It was interesting to observe that the morphologies of nanocomposites changed greatly. The fracture surface can be classified as two parts, one was the fibrillation zone (corresponding to the severely deformed fibrils of the matrix) in the center and the other was the brittle zone at the edges. It can be deduced that the fracture starts near the edges of the sample and propagates inwards. At the same time, the brittle region at the edges and the region close to the fibrillation area were different. For the brittle region at the edges, almost no plastic deformation can be observed. However, brittle region close to the fibrillation zone, some extent plastic deformation can be observed. It can be concluded that when the addition of HNTs is 20 phr, a fracture mode transition from microductility/brittle to brittle/fibrillation occurred. This variation is mainly ascribed to the addition of HNTs, which most likely changes the stress distribution state in the matrix and induces fibrillation/yielding process before crazing.

It is well-known that specimen usually faces complex stress state during the tensile process. Away from the neck zone, tensile stress exhibits the determining role for the deformation of

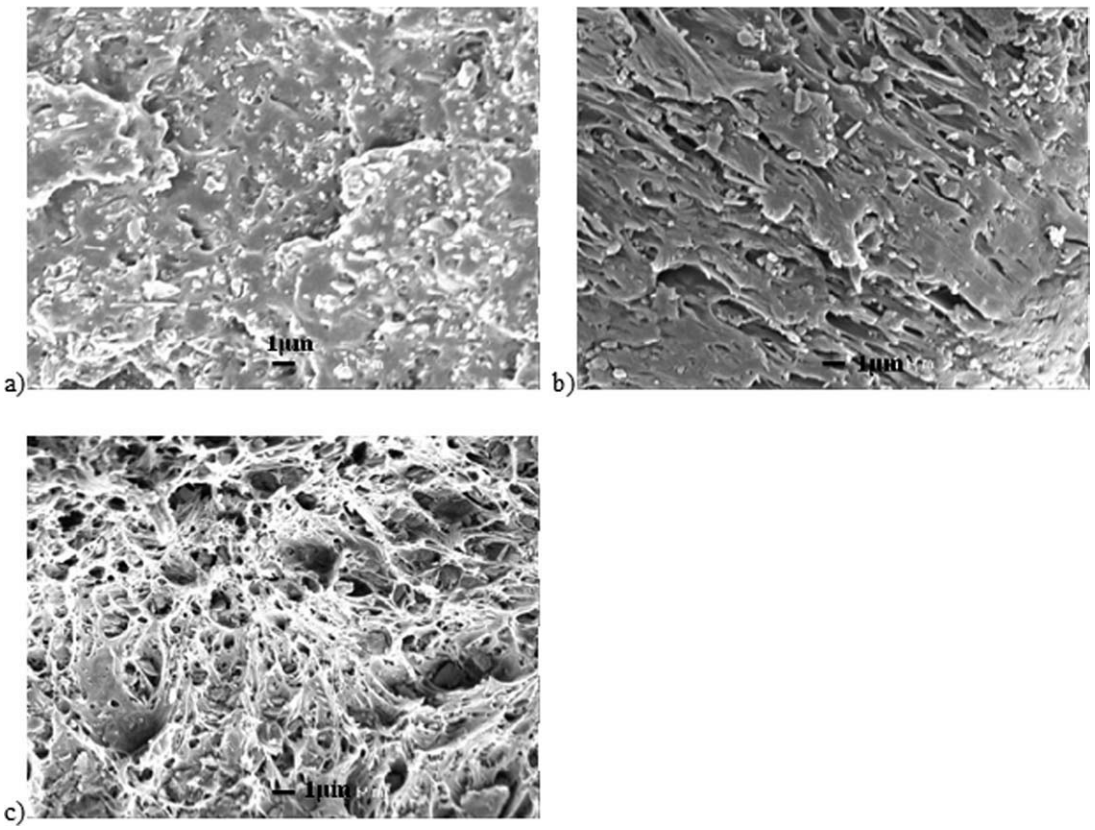

Figure 11. SEM micrograph of the fracture of neat PH_{20} with high magnification from different area: (a) brittle in Figure 10a; (b) brittle in Figure 10b; (c) fibrillation in Figure10(b).

specimen. However in the neck zone, the specimen faces so called triaxial stress including tensile stress, shear stress, and the hydrostatic stress.[29] Generally, the addition of inorganic in polymer would cause two effects: (1) the addition of inorganic particles in the polymer will make the polymer in the vicinity of inorganic particles mechanically restrained[30–35]; (2) The inorganic particles can act as stress concentrators in the polymer matrix and change the stress distribution under an external load.[36,37] Especially during triaxial stress, severe concentration of stress would occur and resulted in restrain strain. In all, the restrained strain would occur with the initiation of the deformation, especially during the triaxial stress stages.

In this research, at low concentration of HNTs, the large matrix ligament thickness can successfully prevent microvoids from developing into premature cracks before the complete yielding of the matrix, so almost no decrease of the elongation at the break was observed. The restrain strain can be released easily. When the concentration of HNTs was 10 phr, the appearance of the HNTs changed the local stress distribution obviously. However, the matrix ligament thickness still can guarantee the sample pass the necking stage, after that, the triaxial stress experienced by sample was released, and the restrain strain can be released too. Therefore, relative good elongation at break was kept for sample PH_{10}. The matrix ligament thickness was so thin when the concentration reached 20 phr, and it cannot guarantee the sample pass the necking stage, so failure happened. With the fracture started near the edges of the sample and propagated inwards, the restrained strain was released, and plastic deformed fibril was observed in the core of the sample.

CONCLUSION

PVDF HNTs nanocomposites were prepared. TEM image showed that the HNTs were almost homogeneously dispersed in PVDF matrix, even at the high concentration of 20 phr. Results showed that the addition of HNTs changed the crystalline structures. For the rheological properties, the qualitative features (shapes) of the viscoelastic behavior were not affected by the introduction of the HNTs, even at the HNTs concentration of 20 phr. However, at a quantitative level, the introduction of HNTs resulted in an increase in the magnitudes of the storage modulus, loss modulus, especially for the sample PH_{20}, a significant increase occurred. The addition of HNTs showed minor effect on the mechanical modulus and fracture behavior at low concentration. However, with the concentration increasing, the mechanical modulus was increased with dramatic decrease of the elongation at break. A fracture mode change from microductility/brittle to brittle/fibrillation occurred when the concentration of HNTs reached 20 phr. This was due to the changing of the stress distribution with the introduction of HNTs.

ACKNOWLEDGMENTS

Mr Tang gratefully acknowledges the support from IPRS (Endeavour International Postgraduate Research Scholarship, Australia), UQRS (University of Queensland Research Scholarship). The authors thank the Arkema for the supply of PVDF free of charge.

REFERENCES

1. Wang, K.; Wang, L.; Wu, J. S.; Chen, L.; He, C. B. *Langmuir* **2005,** *21*, 3613.
2. Wang, K.; Chen, L.; Wu, J. S.; Toh, M. L.; He, C. B.; Yee, A. F. *Macromolecules* **2005,** *38*, 788.
3. Gao, Y.; Li, J. Z.; Liu, L. Q.; Ma, W. J.; Zhou, W. Y.; Xie, S. S.; Zhang, Z. *Adv. Funct. Mater.* **2010,** *20*, 3797.
4. Ma, W. J.; Liu, L. Q.; Zhang, Z.; Yang, R.; Liu, G.; Zhang, T. H.; An, X. F.; Yi, X. S.; Ren, Y.; Niu, Z. Q.; Li, J. Z.; Dong, H. B.; Zhou, W. Y.; Ajayan, P. M.; Xie, S. S. *Nano Lett.* **2009,** *9*, 2855.
5. Arora, A.; Choudhary, V.; Sharma, D. K. *J. Polym. Res.* **2011,** *18*, 843.
6. Ratna, D.; Abraham, T. N.; Siengchin, S.; Karger-Kocsis, J. *J. Polym. Sci. Part B: Polym. Phys.* **2009,** *47*, 1156.
7. Ke, K.; Wen, R.; Wang, Y.; Yang, W.; Xie, B. H.; Yang, M. B. *J. Mater. Sci.* **2011,** *46*, 1542.
8. Ke, K.; Wang, Y.; Yang, W.; Xie, B.-H.; Yang, M.-B. *Polym. Test.* **2012,** *31*, 117.
9. Wen, R.; Ke, K.; Wang, Y.; Yang, W.; Xie, B. H.; Yang, M. B. *J. Appl. Polym. Sci.* **2011,** *121*, 3041.
10. Ke, K.; Wang, Y.; Liu, X.-Q.; Cao, J.; Luo, Y.; Yang, W.; Xie, B.-H.; Yang, M.-B. *Compos. Part B: Eng.* **2012,** *43*, 1425.
11. Liu, M. X.; Guo, B. C.; Du, M. L.; Cai, X. J.; Jia, D. M. *Nanotechnology* **2007,** 182007.
12. Ye, Y. P.; Chen, H. B.; Wu, J. S.; Ye, L. *Polymer* **2007,** *48*, 6426.
13. Ning, N. Y.; Yin, Q. J.; Luo, F.; Zhang, Q.; Du, R.; Fu, Q. *Polymer* **2007,** *48*, 7374.
14. Liu, M. X.; Guo, B. C.; Zou, Q. L.; Du, M. L.; Jia, D. *Nanotechnology* **2008,** 192008.
15. Pasbakhsh, P.; Ismail, H.; Fauzi, M. N. A.; Abu Bakar, A. *Polym. Test.* **2009,** *28*, 548.
16. Dillon, D. R.; Tenneti, K. K.; Li, C. Y.; Ko, F. K.; Sics, I.; Hsiao, B. S. *Polymer* **2006,** *47*, 1678.
17. Patro, T. U.; Mhalgi, M. V.; Khakhar, D. V.; Misra, A. *Polymer* **2008,** *49*, 3486.
18. Hou, M.; Beehag, A.; Yuan, Q. U.S. Pat. 20040231790, **2004.**
19. Bormashenko, Y.; Pogreb, R.; Stanevsky, O.; Bormashenko, E. *Polym. Test.* **2004,** *23*, 791.
20. Pryamitsyn, V.; Ganesan, V. *Macromolecules* **2006,** *39*, 844.
21. Jahani, Y. *J. Vinyl Addit Technol.* **2010,** *16*, 70.
22. Lovinger, A. J.; Wang, T. T. *Polymer* **1979,** *20*, 725.
23. Liu, Z. H.; Marechal, P.; Jerome, R. *Polymer* **1997,** *38*, 4925.
24. Priya, L.; Jog, J. P. *J. Polym. Sci. Part B: Polym. Phys.* **2002,** *40*, 1682.
25. Doyle, M. J.; Orowan, E.; Stork, S. T.; Maranci, A. *Proc. R Soc London Series A: Math Phys Sci* **1972,** *329*, 137.
26. Hadal, R. S.; Dasari, A.; Rohrmann, J.; Misra, R. D. K. *Mater. Sci. Eng. A* **2004,** *372*, 296.
27. Dasari, A.; Misra, R. D. K. *Acta. Mater.* **2004,** *52*, 1683.
28. Hadal, R. S.; Misra, R. D. K. *Mater Sci. Eng. A* **2004,** *374*, 374.

29. Shi, J.; Wang, Y.; Liu, L.; Bai, H. W.; Wu, J.; Jiang, C. X.; Zhou, Z. W. *Mater Sci. Eng. A* **2009,** *512*, 109.
30. Yin, J.; Zhang, Y.; Zhang, Y. X. *J. Appl. Polym. Sci.* **2005,** *97*, 1922.
31. Finnigan, B.; Jack, K.; Campbell, K.; Halley, P.; Truss, R.; Casey, P.; Cookson, D.; King, S.; Martin, D. *Macromolecules* **2005,** *38*, 7386.
32. Fornes, T. D.; Paul, D. R. *Polymer* **2003,** *44*, 4993.
33. Brune, D. A.; Bicerano, J. *Polymer* **2002,** *43*, 369.
34. Folkes, M. J.; Hardwick, S. T. *J. Mater. Sci. Lett.* **1987,** *6*, 656.
35. Maiti, S. N.; Mahapatro, P. K. *J. Appl. Polym. Sci.* **1991,** *42*, 3101.
36. Kim, G. M.; Michler, G. H. *Polymer* **1998,** *39*, 5699.
37. Kim, G. M.; Michler, G. H.; Gahleitner, M.; Fiebig, J. *J. Appl. Polym. Sci.* **1996,** *60*, 1391.